Temperature control of pigsty environment based on improved NFO algorithm and energy-saving priority strategy

Dongya Song*, Wei Yin, Gaoping Wang
School of Mechanical and Electrical Engineering, Xinjiang Institute of Technology, Aksu, 843100, China
*Corresponding author's email: songdya@outlook.com

Abstract: Traditional pigpen temperature control relies on manual adjustments or basic equipment operation, which suffers from significant temperature fluctuations, high energy consumption, and poor uniformity, making it difficult to meet the dynamic needs of pigs at different growth stages. This study proposes an intelligent temperature control optimization method to achieve coordinated optimization of temperature control accuracy, uniformity, and energy efficiency. The research constructs a CFD agent model based on Elman's framework, combined with an improved natural field optimization algorithm. The method employs Tent chaotic mapping to enhance population diversity during initialization, introduces adaptive t-distribution mutation to adjust search step size, and incorporates Pareto strategy to optimize solution sets. Experimental results demonstrate that the improved CFD agent model exhibits excellent temperature prediction performance, achieving an average absolute error of 0.15℃, a coefficient of determination of 0.988, and inference speed of 10.3ms, effectively replacing traditional CFD models for real-time temperature field calculations. In dynamic scenario tests, when pig density varies between 1.0-2.5 heads/m² and the average temperature reaches 27.3℃, the temperature uniformity index remains within a reasonable range of 1.3, with energy consumption increases matching pig density variations. The study reveals that this intelligent temperature control method efficiently balances temperature control accuracy, spatial uniformity, and energy consumption, effectively meeting the dynamic environmental needs of pigs at different growth stages. It provides an efficient and practical solution for intelligent temperature control in large-scale livestock farming scenarios.

Keywords: NFO algorithm; Pigsty temperature; Multi-objective optimization; Energy-saving optimization; Elman neural network

1.Introduction

The stability of the temperature in the pigsty environment directly affects the growth rate and health status of pigs. Traditional control methods rely on manual adjustment or simple equipment start stop, which generally suffer from large temperature fluctuations and high energy consumption, making it difficult to adapt to the environmental needs of pigs at different growth stages [1-2]. Improving the precision and energy efficiency of temperature control in pig pens is an important direction for improving the quality and efficiency of large-scale breeding. Intelligent exploration has emerged in the field of temperature control in pig pens, with some solutions introducing sensors and automatic actuators to achieve basic regulation, or using simple algorithms to optimize equipment operating parameters [3]. But these technologies either focus on controlling a single temperature indicator and ignore the uniformity of internal temperature, resulting in local uneven heating and cooling. Either the convergence speed of the algorithm is slow, and it is difficult to balance temperature stability and energy consumption costs when facing dynamic scenarios such as changes in pig density and external climate fluctuations, resulting in limited energy-saving effects [4-5]. The study proposes an integrated two-layer control framework using an Elman neural network-based Computational Fluid Dynamics (CFD) surrogate model. This model simultaneously outputs energy consumption and temperature metrics to learn low-energy consumption temperature patterns. Combined with an improved Natural Field Optimization (NFO) algorithm employing Pareto strategy, it prioritizes solutions that meet energy consumption targets and temperature control requirements. By dynamically adjusting the water temperature of humidifying curtains and fan speed to reduce redundant energy consumption, the approach aims to enhance precise temperature control and energy-saving optimization.

The innovation of the research lies in constructing an approximate CFD neural network model that integrates Elman feedback mechanism to shorten simulation time. At the same time, the improved NFO algorithm adopts Tent chaotic mapping to enhance the diversity of population initialization, introduces adaptive t-distribution mutation to dynamically adjust the search step size, and combines non dominated sorting to optimize the Pareto solution set distribution. An energy-saving priority wet curtain fan collaborative control strategy is proposed to achieve multi-objective optimization.

2.Related works

The current temperature control in pigsty environments faces the challenges of high energy consumption and low efficiency in traditional regulation methods, and it is difficult to balance temperature uniformity and energy conservation and emission reduction needs. Intelligent optimization strategies are urgently needed to improve energy efficiency and environmental adaptability [6]. J. Lin et al. proposed a multi-objective cooling control optimization method to address the issues of high energy consumption and low management efficiency in hybrid cooling systems for data centers. The results showed that the multi-objective cooling control optimization method significantly reduced the cooling energy consumption in summer and winter, while maintaining the rack cooling index above 95%, effectively improving the energy efficiency and operational safety of data centers [7]. T. M. K. Mohamed et al. proposed an automatic cooling system based on the Internet of Things to address the problem of difficult precise control of root zone temperature and low data acquisition efficiency in traditional pneumatic systems. The results showed that the system could stabilize the root zone temperature at 28.7 ℃-29.2 ℃, significantly better than traditional systems, and effectively optimize the growth environment of aerosol cultivation [8]. L. Wang et al. proposed a nonlinear model predictive control method based on wavelet neural network and improved objective function to address the problem of high energy consumption and difficult balance of control accuracy in greenhouses under low temperature environments in autumn and winter. The simulation results showed that this method reduced energy consumption by 21.02% and 9.54% respectively compared to traditional model predictive control and conventional nonlinear model predictive control, effectively improving the energy efficiency and stability of greenhouse climate control, and providing technical support for sustainable agricultural development [9]. H. Y. Riskiawan et al. proposed an automated control method based on the Internet of Things and artificial intelligence to address the problem of traditional greenhouse environmental monitoring relying on manual operation and low control accuracy. The method used a long short-term memory network model to predict and optimize actuator control. The test results showed that the learning rate of the system was less than 0.002, and it had good predictive ability after 250 steps of training. It could accurately control the actuator based on the data from the first three minutes within three minutes, effectively improving the efficiency of greenhouse environmental regulation and the level of intelligent crop management [10]. A. Zaguia proposed an intelligent greenhouse management system based on the Internet of Things to address the problems of low temperature and humidity control accuracy, redundant data, and difficulty in remote monitoring in traditional greenhouse management. The system combines fuzzy adaptive proportional integral derivative controller and clustering algorithm to optimize environmental regulation. The results showed that the system significantly improved the accuracy of temperature and humidity control and crop yield, reduced energy consumption, and achieved visualization and remote control through cloud platforms and mobile devices, providing an effective solution for intelligent greenhouse management and sustainable agriculture [11]. J. Zhu et al. proposed a method for constructing a temperature and humidity prediction model based on multivariate time series to address the challenges of large temperature and humidity fluctuations and delayed response of environmental control equipment in enclosed pigsties. Pearson correlation analysis and normalization were used to screen input features, and the performance of multiple models was compared. The results showed that the hybrid model combining dynamic directed graph convolution and recurrent neural network had the highest prediction accuracy, and this model could provide early warning and decision support for precise control of pigsty environment [12].

S. The Li team proposed a random data fusion network deployment method based on multi-objective optimization to address the problem of poor practical application results caused by model simplification in wireless sensor network deployment, and designed an enhanced multi-objective mongoose optimization algorithm. The simulation results showed that the algorithm outperformed traditional multi-objective algorithms in terms of optimization performance and convergence, and has good potential for application [13]. R. Xing proposed a variable air volume ventilation control method based on conservation equations and first-order delay models to address the issues of low precision and high energy consumption in tunnel ventilation systems. A dynamic airflow control model was established to solve the relevant parameters and transfer functions. The experimental results showed that this method could effectively achieve dynamic adjustment of wind speed, and the control system had good response performance. The overshoot, steady-state value, and adjustment time were all within the error range, and it had good energy-saving effect and application value [14]. H Yang et al. proposed a relationship model between the optimal temperature difference, environmental dew point temperature, and compressor frequency in a variable frequency dehumidification system, based on the control index of dehumidification operation temperature difference, to address the problems of difficult coordinated control of compressor frequency and fan speed, and limited dehumidification performance. The experimental results showed that this method could effectively optimize dehumidification capacity and energy efficiency, with a maximum deviation of only 5.97%, providing efficient frequency conversion control strategies and logical design guidance for virtual file directory systems [15]. V. Dhakane et al. proposed a machine learning model that combines CFD and deep neural networks to address the complex multiphase fluid dynamics behavior and high computational costs of traditional simulations in bubble column reactors. The results showed that the prediction accuracy determination coefficient reached 0.97-0.99, and a graphical interface was developed to improve model usability, significantly reducing simulation costs and time, providing an efficient and accurate new method for the design optimization of bubble column reactors [16].

In summary, the current greenhouse environment temperature control faces the problems of high energy consumption, low efficiency, and difficulty in balancing temperature uniformity with energy conservation and emission reduction. The study constructs a CFD model based on Elman-NN, introduces an improved NFO algorithm, enhances initial population diversity through Tent chaotic mapping, dynamically adjusts the search process through adaptive t-distribution mutation strategy, and uses non dominated sorting mechanism to improve solution set quality. Implementing multi-objective optimization aims to improve the energy efficiency and environmental stability of pig pens, and solve the drawbacks of traditional temperature control.

3.Methods and Materials

3.1 Energy-saving priority strategy for CFD model based on Elman-NN

In terms of temperature control in pigsty environments, traditional methods have many limitations and are difficult to accurately regulate, resulting in the susceptibility of pig herds to temperature fluctuations, slow growth, and frequent disease outbreaks [17]. Although modern technology has achieved a certain degree of automatic adjustment and can control ventilation and temperature control equipment based on temperature sensor data, it still cannot achieve efficient and accurate control in the face of complex and changing environments. With the development of technology, neural networks have brought about a revolution in CFD, effectively improving the accuracy and efficiency of CFD simulations [18-19]. Due to the time required for CFD calculations of heat transfer and flow, a single run time is usually 5-8 hours. Multi-objective optimization algorithms require at least thousands of searches in the solution space during the optimization process, and directly using CFD models will consume a lot of time and computational resources [20]. Neural networks can accurately capture the complex airflow and temperature distribution patterns in pigsty by learning from large amounts of data, greatly reducing simulation time and optimizing simulation results. Therefore, the introduction of neural network approximation models can reduce the number of high-intensity simulation calculations in computers. The construction of the neural network approximation model is shown in Figure 1.

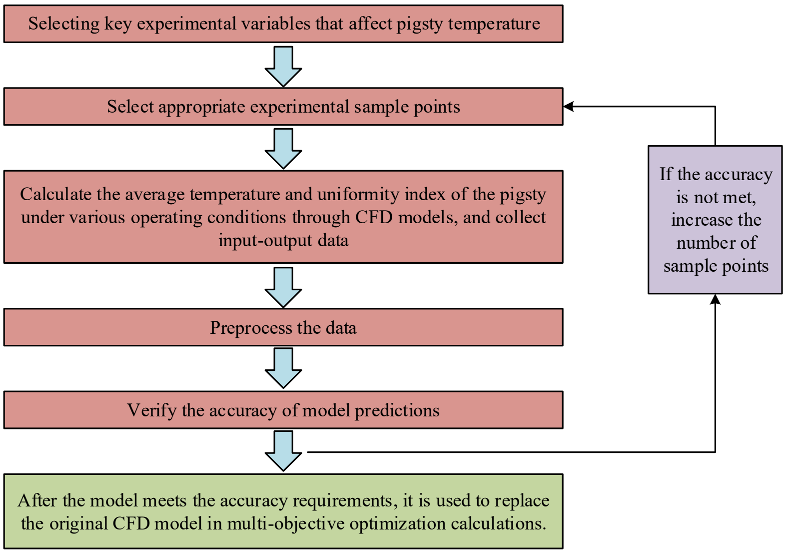

Figure 1 Schematic diagram of constructing approximate neural network model

According to Figure 1, the model first needs to determine the key variables and factors that affect the temperature response of the pigsty. Then, the experimental design method is used to generate typical working condition samples, and data is obtained through CFD simulation to construct a neural network proxy model. If the verification accuracy meets the standard, replace the CFD model; otherwise, increase the sample size and re model. The core of this process lies in approximating complex CFD models by constructing simplified proxy models, improving the efficiency of optimization control, making it practical in engineering, and providing an efficient approach for calculating the objective function in subsequent multi-objective optimization algorithms. The neural network approximation model can quickly predict the temperature indicators of pigsty under different variables, providing an efficient tool for pigsty cooling regulation [21]. The core principle of cooling pigsty in summer is to use the physical phenomenon of "water evaporation absorbing heat", but the actual cooling effect is affected by various factors such as environmental temperature, humidity, and ventilation efficiency [22]. By studying the cooling mechanism of pigsty, the design of cooling system can be optimized to achieve more efficient temperature control effect. The cooling principle of the pigsty is shown in Figure 2.

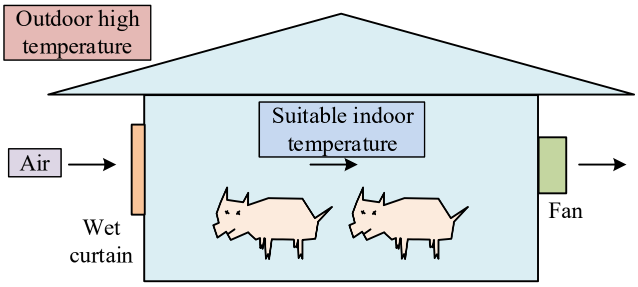

Figure 2 Cooling principle of pigsty

According to Figure 2, the core of the summer cooling system in the pigsty lies in the coordinated operation of the wet curtain and fan. As the generation end of cold air, the wet curtain is installed at one end of the pigsty. The water on its surface is in full contact with the incoming hot air, and when the water evaporates, it absorbs a large amount of heat, converting the hot air into cooler cold air. The cooling efficiency of the wet curtain directly affects the temperature of the air entering the pigsty. The calculation of the air temperature of the wet curtain is shown in equation (1).

$$W_i = W_o - \beta(W_o - W_d) \qquad (1)$$

In equation (1), W_i represents the temperature at which air enters the pigsty through the wet curtain, W_o represents the outdoor air temperature, β represents the cooling efficiency of the wet curtain, and W_d represents the temperature of the wet curtain spray water at the air inlet. The control of water temperature in the wet curtain is crucial for the cooling effect, such as using ice water or groundwater to spray the wet curtain at high temperatures, which can achieve lower temperature intake. The fan is installed at the end opposite to the wet curtain, and when it operates, it extracts the air inside the building, creating a pressure difference between the inside and outside of the building, and promoting the continuous entry of cold air cooled by the wet curtain into the building. At the same time, the air that has absorbed the metabolic heat of pigs is discharged, and the outlet wind speed of the fan is a key parameter. The cooling of pig houses requires a combination of multiple factors such as temperature, humidity, and ventilation, achieved through principles such as evaporation and convection. However, dynamic changes in the environment can easily lead to fluctuations in the cooling effect [23]. To accurately model and optimize cooling and energy-saving strategies, it is necessary to introduce intelligent algorithms that can handle time-series data and nonlinear relationships. Elman-NNs, with their feedback mechanism and dynamic learning ability, can effectively adapt to this demand. The Elman-NN structure is shown in Figure 3.

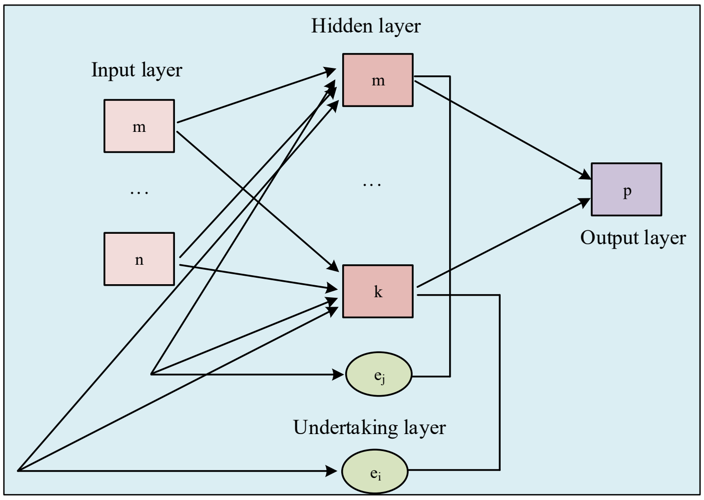

Figure 3 Elman-NN structure

Based on the Elman neural network structure shown in Figure 3, the CFD neural network incorporating Elman's framework was developed. It specifies outdoor temperature, pig density, wet curtain water temperature, fan speed, and indoor humidity as key experimental inputs for pig houses, with the average temperature and spatial temperature difference coefficient of the breeding house serving as core evaluation metrics. Among them, the average temperature is calculated by summing and averaging the temperatures at multiple observation points above the pigsty, as shown in equation (2).

$$\overline{W} = \sum_{m=1}^{k} w_m / k \qquad (2)$$

In equation (2), $\overline{W}$ represents the average temperature inside the pigsty, w_m represents the temperature value of the m th observation point inside the pigsty, and k represents the number of observation points. The temperature difference coefficient is calculated by taking the square root of the deviation between the temperature at each observation point and the average value, as shown in equation (3).

$$W' = \sqrt{\frac{1}{k}\sum_{m=1}^{k}\left(\overline{W} - w_m\right)^2} \qquad (3)$$

In equation (3), W' represents the temperature difference coefficient inside the pigsty. Then, the data is normalized to adjust the input signal to a uniform numerical level to avoid neuron training saturation, and the output is restored to the actual value through inverse normalization, as shown in equation (4).

$$z_m = (z_{ax} - z_{in})z_m^{'} + z_{in} \qquad (4)$$

In equation (4), z_{ax} and z_{in} are the maximum and minimum values of the input data, z_m is the actual predicted value output by the network model, and $z_m^{'}$ is the normalized result. The receptive layer of the neural network is responsible for memorizing the hidden layer output of the previous time step, enabling the model to better capture the dynamic changes in pigsty temperature. The number of hidden layer nodes can be determined by calculation, as shown in equation (5).

$$Y_l = \sqrt{(i+j)} + e \qquad (5)$$

In equation (5), Y_l represents the number of hidden layer neurons, i represents the number of nodes in the data receiving layer, j represents the number of nodes in the data transmitting layer, and e is a constant between 1 and 10. The approximate model designed for research can efficiently map the complex nonlinear relationship between design parameters and temperature fields, significantly improving computational efficiency and effectively replacing CFD models for real-time calculation of multi-objective optimization. It can solve the problems of complex calculation and long convergence time of CFD models [24].

3.2 Improved NFO algorithm model

The energy-saving strategy based on Elman-NN CFD model can quickly simulate the temperature field of pigsty, improve simulation efficiency and accuracy, provide efficient calculation methods for multi-objective optimization, and help balance temperature control and energy consumption. To assist in better parameter optimization and achieve coordinated optimization of temperature precision control and energy saving, an improved NFO algorithm model is proposed based on optimized CFD energy-saving strategies, which improved optimization efficiency through dynamic neighborhood search and adaptive weight mechanism [25-26]. The algorithm process is shown in Figure 4.

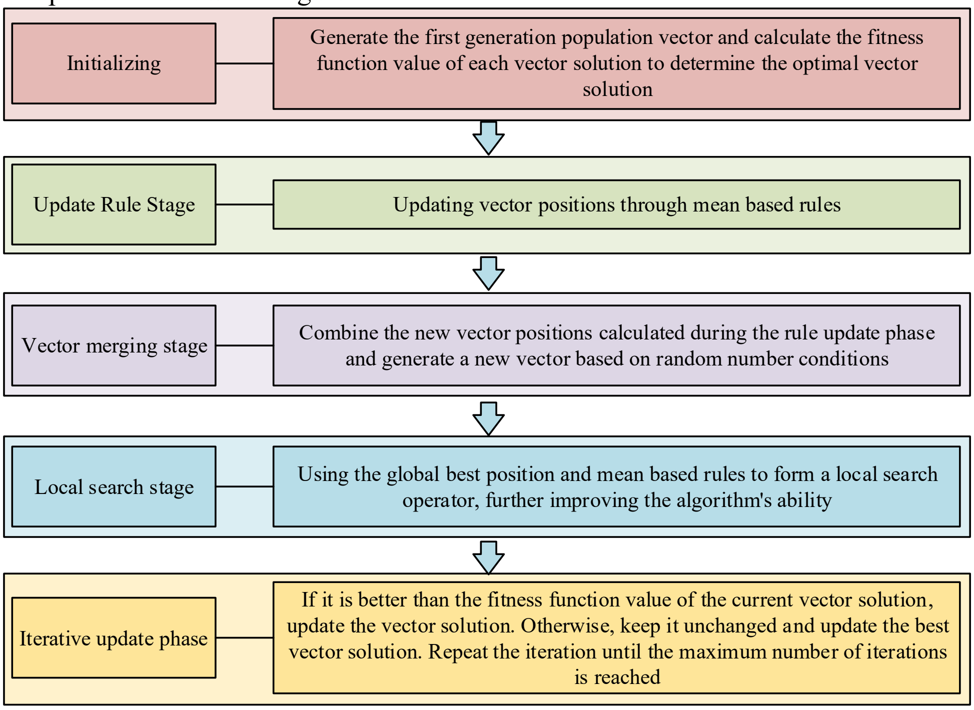

Figure 4 NFO algorithm principle process diagram

According to Figure 4, this principle mainly includes initialization, updating rules, vector merging, and local search. Firstly, initialization is performed by randomly initializing individuals in the search space to generate the first generation population vector. Then, the position of the vector is updated using a mean-based rule, and the direction of movement is determined by weighting the central trend of the random vector set. To enhance global exploration performance, an adaptive acceleration mechanism is incorporated into the position update equation, with core parameters including dynamically adjusted vector scaling coefficients and time-varying weight factors. At the same time, introducing a random integer sampling mechanism to participate in the calculation process effectively maintains the diversity characteristics of the population [27]. In the vector merging stage, the positions of two new vectors calculated in the update rule stage are combined to generate new vectors based on specific conditions. This step is used to improve local search capabilities and provide more promising vectors. Finally, in the local search stage, a new search operator is constructed by integrating the global optimal solution with the mean guided strategy to finely adjust the candidate solutions, thereby enhancing the convergence accuracy and optimization efficiency of the algorithm [28-29]. To optimize the NFO algorithm and achieve hierarchical solutions in multi-objective optimization, the study introduces fast non-dominated sorting to determine dominance relationships, which helps the NFO algorithm efficiently screen high-quality solutions. The algorithm flow of non dominated sorting is shown in Figure 5.

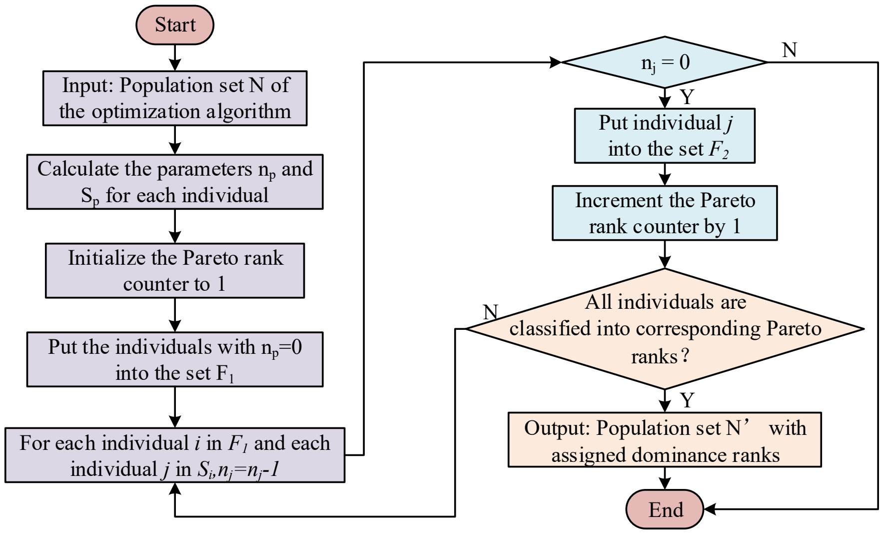

Figure 5 Non-dominated sorting algorithm flowchart

According to Figure 5, the process begins with population input, first calculating the number of dominations and the set of dominated individuals for each individual, which is the basic data for subsequent stratification. After initializing the level counter, the algorithm classifies all individuals that are not dominated by any solution into the first layer elite set F_1, and these individuals constitute the current optimal solution set. When dealing with individuals in F_1, the algorithm will traverse all the individuals it governs and reduce their domination frequency. If the dominance frequency of an individual becomes 0 as a result, it will be added to the next elite set F_2. After completing F_1 processing, the algorithm processes F_2 and subsequent levels in the same way until all individuals are stratified. This hierarchical structure is particularly suitable for multi-objective optimization problems of large-scale populations, providing an efficient and reasonable basis for individual sorting in subsequent selection operations [30]. Based on the above algorithm mechanism, an improved NFO algorithm is proposed, which integrates chaotic mapping initialization population to enhance traversal, introduces adaptive t-distribution mutation operator to dynamically adjust search step size, and draws on non dominated sorting strategy to maintain Pareto solution set distribution . The improved NFO algorithm process is shown in Figure 6.

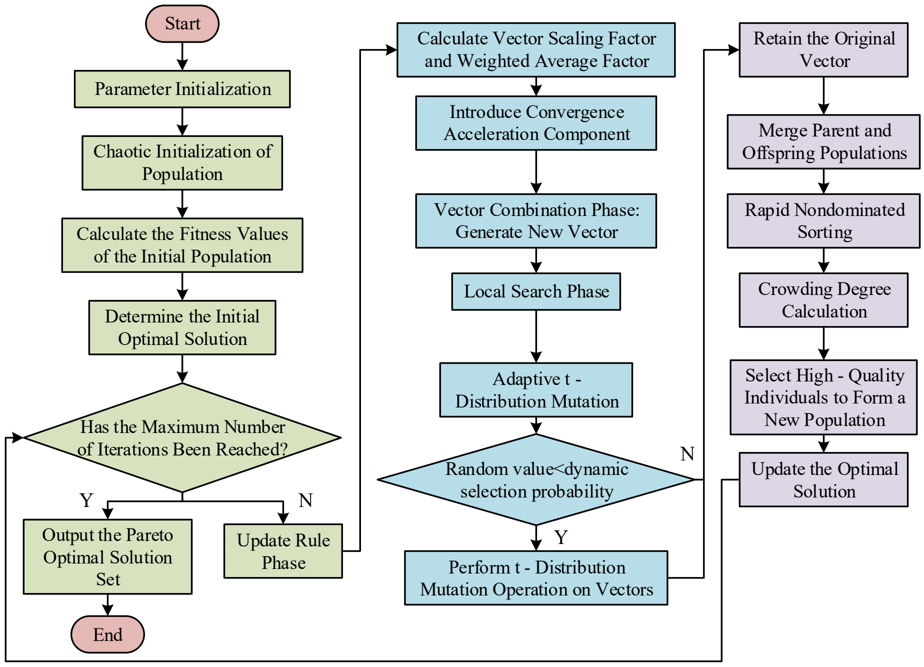

Figure 6 Improved NFO algorithm flowchart

According to Figure 6, the newly generated algorithm flowchart starts with parameter initialization. After setting basic parameters such as population size and maximum iteration times, chaos initialization is performed through chaos mapping to generate uniformly distributed initial solution vectors. Then, the fitness of each vector is calculated and the initial optimal solution is determined. The chaos mapping formula is shown in equation (6).

$$C_{a+1} = M(C_a + 0.2 - (\frac{0.5}{2\pi}) \times sin(2\pi C_a), 1) \qquad (6)$$

In equation (6), C_{a+1} represents the next chaotic variable value generated after mapping, C_a represents the current chaotic variable value, and M represents the modulo operation, which is used to limit the calculation result to the [0,1] interval. Subsequently, it enters an iterative loop where two new vectors are generated during the rule update phase. During this phase, the vector scaling rate and weighted average factor are calculated. The fused weighted average rule is then introduced into the convergence acceleration section, and a new vector is generated during the vector combination phase. The update of the vector solution is shown in equation (7).

$$T=NZ+NZ*tr(d) \qquad (7)$$

In equation (7), T represents the temporary position or temporary state value of the individual after this update operation, NZ represents the new position vector or new state parameter value obtained by the individual, tr represents a random number generation function between 0 and 1, and d represents the number of iterations. Subsequently, the newly generated vector is optimized using the global best position during the local search phase, followed by adaptive t-distribution mutation, as calculated in equation (8).

$$L = 1 - exp(1 - \frac{d}{Md})^{0.5} + 0.5 \qquad (8)$$

In equation (8), L represents the dynamic selection probability, d represents the current iteration count, Md represents the maximum iteration count, and $\exp$ represents the natural exponential function. Next, the original vectors retained from the parent and offspring populations are merged, and the Pareto hierarchy is divided using fast non-domination sorting. Crowding is calculated to maintain population diversity, and high-quality individuals are selected to form a new population and update the key solution until the maximum number of iterations is reached, at which point the Pareto optimal solution set is output. The improved NFO algorithm enhances global search capabilities and convergence speed, effectively handling multi-objective optimization problems .

4.Results

4.1 Experimental environment and data sources

The simulation experiment dataset used in the study integrates actual monitoring data and CFD simulation results, based on the environmental monitoring data of a large-scale pigsty in Shandong Province for the whole year of 2022, including key parameters such as temperature, humidity, and CO_2 concentration. The sampling interval was 5 minutes, covering different working conditions throughout the four seasons. At the same time, the operation status and energy consumption data of fans, wet curtains, and underfloor heating equipment were synchronously collected to ensure measurement accuracy is controlled within plus or minus 2%. The CFD benchmark model was constructed using ANSYS Fluent and a 3D pigsty model with 1.2 million grids was used. The simulation error of the velocity field was verified to be less than 8% through actual testing. To optimize and improve the input features of NFO algorithm, the dataset further integrated 12 dimensional derived features such as temperature gradient and heat load index. By introducing positive and negative 10% noise perturbations to enhance data robustness, a complete dataset containing 8760 hours of standardized time-series data was ultimately formed. NSGA-II uses a population size of 50, crossover probability of 0.9, and mutation probability of 0.01. MOPSO employs 50 particles with linearly decreasing inertia weights (0.5-0.9) and a learning factor of 2.0. PID features a proportional coefficient of 2.5, an integral coefficient of 0.3, and a derivative coefficient of 0.1. At the same time, to verify the performance of the improved NFO model and neural network approximation model combined with the research, experiments were conducted on the Ubuntu 20.04 LTS operating system. The specific configuration of the experimental environment is shown in Table 1.

Table 1 Detailed information of the testing platform

-	Configure	Parameter
Hardware configuration	CPU	Intel Xeon Gold 6348
	GPU	NVIDIA A100
	Storage	2TB NVMe SSD+ 10TB HDD
	Motherboard	Intel W790
Software configuration	Operating system	Ubuntu 20.04 LTS
	CFD simulation software	ANSYS Fluent 2023 R2
	Programming language tools	Python 3.9+
	Multi objective optimization library	pymoo 0.6.0
	Data processing tools	Pandas 1.5+
	Visual Tools	Matplotlib 3.7+

4.2 Experimental results of energy-saving priority strategy for CFD approximate model

All algorithms were executed on an Ubuntu 20.04 L TS system with an Intel Xeon Gold 6348 CPU and NVIDIA A100 GPU. The control parameters included a pigpen measuring 28m×13m, a monitoring height of 1.2m, and a sampling interval of 5 minutes. The simulated experiment was conducted at an ambient temperature range of 30℃-40℃, covering typical summer high-temperature conditions. This experiment aims to investigate the effect of wind speed at the outlet of the fan on temperature changes in the pigsty. Observation points M1 and M2 near the fan end were selected to compare the dynamic temperature changes under experimental wind speeds of 1m/s (A1), 3m/s (A2), and 5m/s (A3), to analyze the impact of wind speed on cooling rate and stable state. The test results are shown in Figure 7.

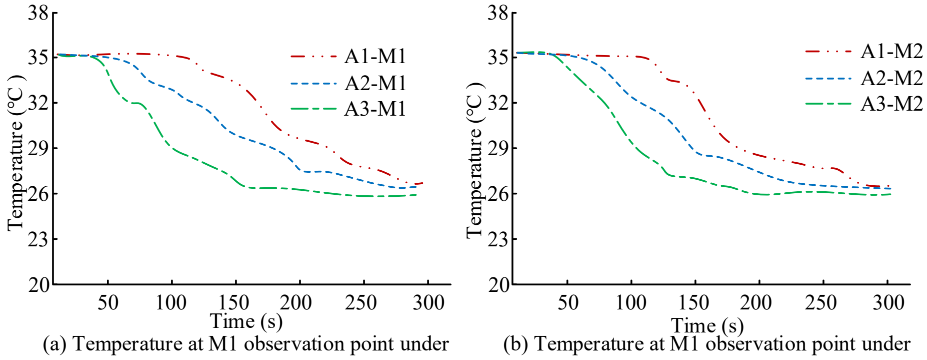

(a) Temperature at M1 observation point under different wind speeds

(b) Temperature at M1 observation point under different wind speeds

Figure 7 Dynamic temperature at observation points in pig houses under different fan outlet wind speeds

According to Figure 7 (a), due to the effect of the exhaust system, the temperature of the pigsty decreased to a certain temperature over time. At A3 wind speed, the temperature at the observation point began to decrease earlier and at a faster rate. It reached a stable temperature at 150S, and the final stable temperature was about 26 ℃. The higher the wind speed, the lower the temperature reached. The cooling of A1 wind speed lagged behind, and the stable temperature was relatively high, about 27.4 ℃. According to Figure 7 (b), the temperature change trend at observation point M2 was roughly the same as that at observation point M1. However, the faster the temperature dropped at observation point M2, the faster the wind speed at A3 reached about 26 ℃, A2 reached about 26.4 ℃, and A1 reached about 26.6 ℃. Therefore, the higher the wind speed of the fan, the stronger the negative pressure formed, which promotes the wet curtain cold air to flow faster through various areas inside the pigsty, accelerates heat exchange, shortens the cooling response time, and at the same time, high wind speed can more efficiently carry away the heat of the pigsty, making the temperature inside the pigsty reach a lower stable state faster. However, at low wind speeds, the air flow is slower, and heat accumulation weakens the cooling effect. The experiment aimed to investigate the effect of the intake temperature at the wet curtain on the temperature inside the pigsty. Observation points M1 and M2 were selected to compare the temperature changes of the intake temperature at 22 ℃ (B3), 23 ℃ (B2), and 24 ℃ (B1), and analyze the effect of the intake temperature on the cooling effect. The test results are shown in Figure 8.

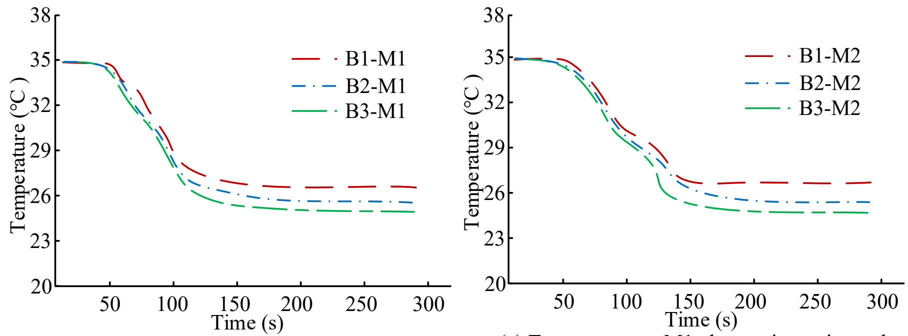

(a) Temperature at M1 observation point under different wind speeds

(a) Temperature at M1 observation point under different wind speeds

Figure 8 Air intake temperature of wet curtain and temperature variation at observation point

According to Figure 8 (a), in B3, the temperature at the observation point dropped earlier, with a slightly steeper downward trend than B1 and B2. The final stable temperature was lower, about 25 ℃, and the temperature difference with B1 continued to expand over time. Finally, the temperature of B1 stabilized at about 27.4 ℃. At the same time, the time for different intake temperatures to reach a stable temperature was basically within 100 seconds. According to Figure 8 (b), the temperature change trend at observation point M2 was slightly different from that at point

M1. It took about 150 seconds for the exhaust temperature at observation point M2 to reach a stable temperature, and the temperature dropped faster between 50-80 seconds, and slower between 80-150 seconds. The stable temperatures reached at the inlet temperatures of B1, B2, and B3 were approximately 27 ℃, 25.7 ℃, and 24.9 ℃, respectively. The lower the intake temperature, the more cooling capacity it carries, and the stronger the ability to absorb heat inside the pigsty after entering, which can effectively reduce the ambient temperature inside the pigsty. At the same time, low-temperature air can still maintain a lower final temperature after flowing through the pigsty and interacting with factors such as heat production by the pigs, while higher intake temperatures have a weaker cooling effect due to insufficient initial cooling capacity, resulting in a significant difference in the final stable temperature between the two. To optimize the location of environmental monitoring points in the pigsty, based on CFD simulation analysis of the environmental distribution during summer wet curtain fan cooling, five monitoring nodes were arranged in a 28 meter long and 13 meter wide fattening pigsty to better collect environmental parameters inside the pigsty. The optimization results are shown in Figure 9.

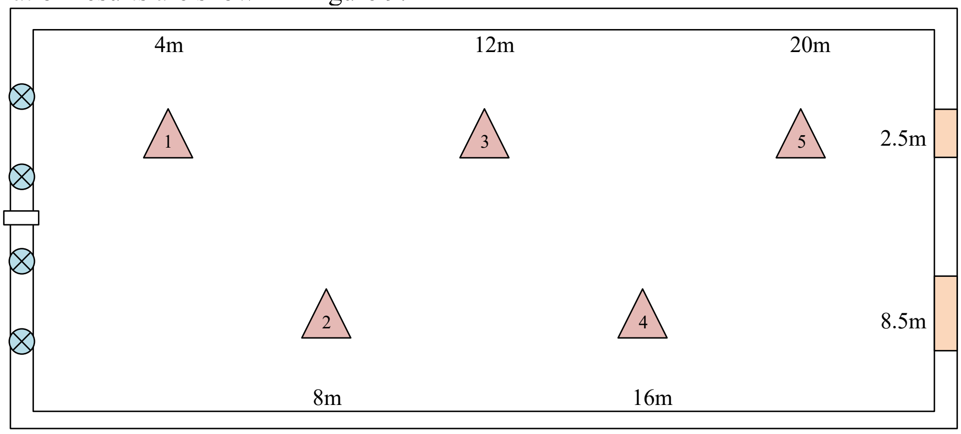

Figure 9 Optimized layout of five monitoring nodes for wet curtain-fan cooling system

According to Figure 9, the five monitoring nodes were asymmetrically distributed in the pig living area on both sides of the middle aisle, with a height of 1.2 meters, avoiding the aisle, wet curtains, and areas near the fan. From the layout effect, this arrangement could effectively avoid areas with large airflow disturbances, such as wet curtains and fans, where local parameter fluctuations were caused by ventilation, and corridors were prone to temperature changes due to external airflow. The selected nodes were located in the core area of pig activity, which can accurately reflect the true state of the pig's living environment. Based on CFD simulation analysis, the ventilation system of the pigsty was symmetrical but there were slight differences in environmental distribution. Asymmetric arrangement could cover more diverse microenvironments. The height of 1.2 meters was close to the activity level of pigs and avoided the obstruction of airflow by the pigsty, ensuring the representativeness of monitoring data. At the same time, reducing the number of nodes could lower hardware costs and energy consumption, balancing monitoring effectiveness and economy. The experiment aimed to evaluate the performance of different neural network models in simulating the temperature field distribution of CFD, and compare the differences in temperature prediction accuracy, training efficiency, and inference speed among the CFD benchmark model, the original Elman-NN model, the Long Short Term Memory (LSTM), the Gated Recurrent Unit (GRU), and the improved Elman-NN model (represented by GElman-NN). The test results are shown in Table 2.

Table 2 Performance of Different Neural Network Models in Simulating CFD Temperature Field Distribution

Model type	MAE(℃)	RMSE(℃)	R^2	Training time (h)	Inference speed (ms)
CFD benchmark	0.00	0.00	1.000	-	23400000
Elman-NN	0.18	0.24	0.983	0.63	12.5
LSTM	0.23	0.31	0.972	1.87	47.8
GRU	0.21	0.28	0.978	1.60	39.2
GElman-NN	0.15	0.20	0.988	0.75	10.3

From Table 2, each model exhibited significant differences in simulating the CFD temperature field. The Mean Absolute Error (MAE) of GElman-NN was 0.15 °C, and the Root Mean Square Error (RMSE) was 0.20 °C, which is superior to Elman-NN, LSTM, and GRU in terms of indicators. The coefficient of determination (R-Squared, R^2) value was 0.988, and its temperature prediction accuracy was closest to the CFD benchmark model. In terms of training efficiency, GElman-NN had a training time of 0.75 hours, slightly higher than Elman-NN, but much lower than LSTM's 1.87 hours and GRU's 1.60 hours, achieving a good balance between accuracy and efficiency. In terms of inference speed, GElman-NN was 10.3ms. Due to the enhanced dynamic modeling ability through feedback connections, GElman-NN maintained high inference efficiency. Overall, GElman-NN performs the best in comprehensive performance, maintaining high accuracy while maintaining fast training and inference speed, making it suitable for real-time temperature field prediction applications.

4.3 Performance testing of improved NFO algorithm

To evaluate the temperature control performance of the proposed "enhanced NF algorithm + Elman-CFD agent model" under typical operating conditions, this study compares it with mainstream algorithms (PID, MPC, and traditional GA-CFD) in terms of temperature control accuracy, energy optimization, temperature uniformity, and dynamic response. Using a 28m×13m large-scale pigpen in Shandong as the prototype, the experiment set the outdoor temperature at 35°C and pig density at 1.5 heads/m² as standard variables. The daily energy consumption refers to the total energy consumption of the temperature control system (including wet curtain and fan) in a single 28m×13m pigpen. Non-temperature control equipment is excluded. The installation position of the power meter, sampling interval, and 24-hour cumulative statistical method are supplemented, with test results presented in Table 3.

Table 3 Comparison of Core Performance Metrics for Pigsty Temperature Control Using Different Algorithms

Algorithm Type	MAE(°C)	RMSE(°C)	Daily Average Energy Consumption (kWh)	Temperature Difference Coefficient	Response Time (s)
PID	0.68	0.85	91.40	2.30	270
MPC	0.42	0.58	83.70	1.90	210
Traditional GA-CFD Integration	0.35	0.45	77.50	1.60	180
Research Methodology	0.18	0.25	68.90	1.10	140

As shown in Table 3, the study method demonstrates optimal temperature control accuracy (MAE: 0.18°C, RMSE: 0.25°C) under outdoor conditions of 35°C and a pig density of 1.5 heads/m², significantly outperforming comparative methods. This advantage stems from the Elman-CFD surrogate model's precise capture of complex airflow and temperature distribution patterns in pig houses. The enhanced NFO algorithm employs Tent chaos mapping to boost population diversity and adaptive t-distribution variation to adjust search step sizes, achieving efficient parameter optimization. With daily energy consumption of 68.9kWh—lower than PID's 91.4kWh, MPC's 83.7kWh, and traditional GA+CFD's 77.5kWh—the system achieves this through coordinated regulation of wet curtain water temperature and fan speed under an energy-saving priority strategy. The temperature difference coefficient (1.1) remains within reasonable limits, while the response time of 140s surpasses the traditional GA+CFD's 180s. The optimized temperature field uniformity in the GA+CFD algorithm and the surrogate model's computational efficiency effectively address core challenges in traditional temperature control systems.To verify the temperature control effect of the improved NFO, the distribution characteristics of temperature mean square error and energy consumption of Non-dominated Sorting Genetic Algorithm II (NSGA-II), Multi-Objective Particle Swarm Optimization (MOPSO) algorithm, and Proportional-Integral-Derivative-Control (PID) were compared to verify the robustness of the improved NFO. The test results are shown in Figure 10.

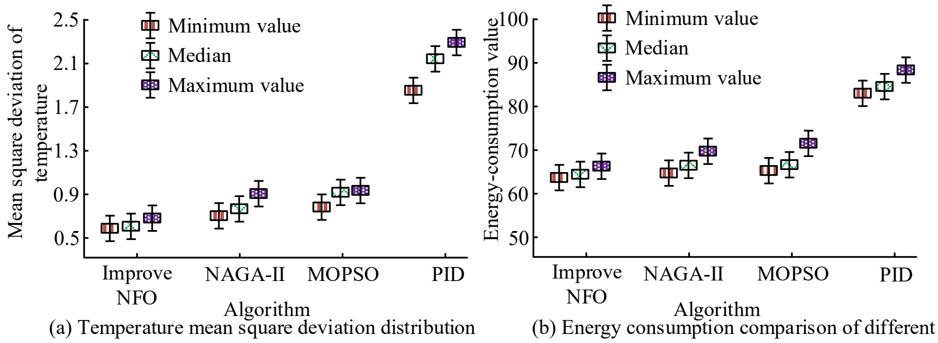

(a) Temperature mean square deviation distribution of different algorithms (b) Energy consumption comparison of different algorithms

Figure 10 Performance Comparison of Different Algorithms

According to Figure 10 (a), the improved NFO algorithm was significantly superior to other algorithms in terms of the minimum, median, and maximum values of temperature mean square error. Its minimum value was 0.63, median was 0.68, and maximum value was 0.75, which was lower than NSGA-II and MOPSO. It differed the most from the minimum, median, and maximum values of PID, which were 1.32, 1.47, and 1.6, respectively. The improved NFO algorithm performed well in temperature control accuracy and stability because it can more accurately find the optimal solution for temperature control by optimizing the search strategy, and has strong robustness and adaptability, which can maintain good temperature control effects in various complex environments. According to Figure 10 (b), the improved NFO algorithm was significantly lower than other algorithms in terms of minimum, median, and maximum energy consumption. Its minimum value was 64.2, median was 65.7, and maximum value was 67.8, significantly lower than NSGA-II, MOPSO, and PID. Due to the improved NFO algorithm fully considering energy consumption factors during the optimization process, it could reduce energy consumption while ensuring temperature control effectiveness. When the temperature mean square error decreases from 0.5℃ to 0.25℃, the energy consumption only increases from 72kWh to 75kWh, an increase of 4.2%; while the energy consumption of the traditional algorithm increases by more than 15% when the error is reduced by the same amount, indicating that the algorithm can achieve significant improvement in temperature control accuracy with low energy consumption increment. The experiment selected $f_1(x)=\sum_{i=1}^{n} x_i^2$ and $f_2(x)=\sum_{i=1}^{n}|x_i|+\prod_{i=1}^{n}|x_i|$ as benchmark functions to compare the performance of the improved NF algorithm, the original NF algorithm, and the original particle swarm optimization algorithm. The convergence curves were used to evaluate the differences in convergence accuracy, speed, and ability to escape local optima. The test results are shown in Figure 11.

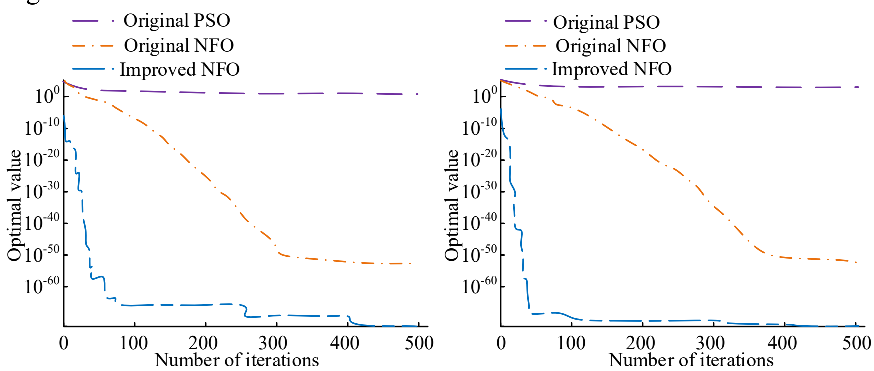

(a) Function 1 test results (b) Function 2 test results

Figure 11 Comparison of results of different benchmark test functions

According to Figure 11 (a), the improved NFO algorithm showed a faster downward trend from the initial iteration, with the function value dropping below 10^{-50} after 50 iterations and tending to below 10^{-60} after 100 iterations. The original NFO algorithm decreased slowly, with a function value of about 10^{-50} after 300 iterations. The original PSO algorithm converged the slowest, with a final value of only about 10^{-5}. This result is due to the chaos initialization of the improved algorithm, which makes the population distribution more uniform and can quickly approach the optimal solution region. The adaptive t-distribution mutation expanded the search range with a large mutation amplitude in the early stage of iteration, and reduced the mutation amplitude for fine optimization in the later stage. Therefore, it combined global search efficiency and local convergence accuracy on unimodal functions. According to Figure 11 (b), the improved NFO algorithm in the figure reduced the function value to below 10^{-60} after 50 iterations, and the value reached stability and was at its minimum after 400 iterations. After 370 iterations of the original NFO algorithm, the function value was about 10^{-50}, while the final value of the original PSO algorithm was only about 10^{-3}. The multi-layer nested structure of this function required higher local mining capabilities for the algorithm. The improved algorithm introduced non-dominated sorting and crowding calculation to reduce redundant searches. Combined with the global exploration of chaotic mapping and local development of t-distribution variation, it could efficiently locate the optimal solution in complex unimodal spaces. However, the original algorithm is prone to falling into local suboptims, and the PSO algorithm lacks mutation mechanism, resulting in insufficient convergence power in the later stage. The experiment was based on an improved NFO algorithm and energy-saving priority strategy. By dynamically adjusting the water temperature of the wet curtain and the wind speed of the fan through the improved NFO algorithm, the changes in temperature and energy consumption under different densities were explored to verify the algorithm's adaptability to dynamic environments. The test results are shown in Figure 12.

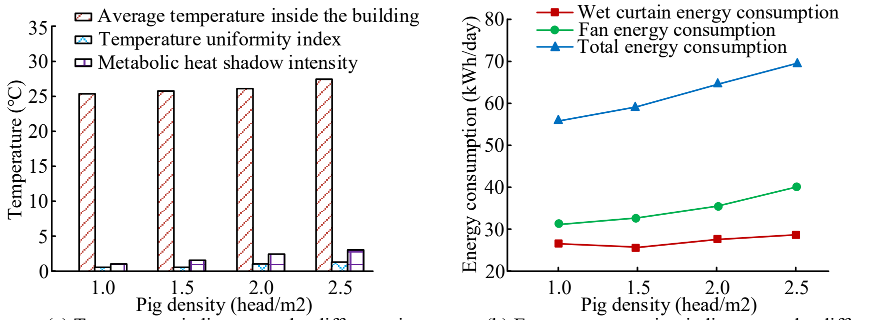

(a) Temperature indicators under different pig densities

(b) Energy consumption indicators under different pig densities

Figure 12 Control effect under different pig densities

According to Figure 12 (a), as the pig density increased from 1.0 head/㎡ to 2.5 head/㎡, the average temperature inside the house increased from 25.2 °C to 27.3 °C, the temperature uniformity index increased from 0.8 to 1.3, and the metabolic heat impact degree increased from 1.2 °C to 3.3 °C. The reason is that as the density increases, the total metabolic heat production of pigs increases, and the accumulation of heat in the shed accelerates, resulting in an increase in average temperature. At the same time, local heat concentration became more pronounced, temperature distribution uniformity decreased, and the impact of metabolic heat on environmental temperature increased accordingly. Although the improved NFO algorithm dynamically adjusted the equipment, it was difficult to completely offset the heat generation increment under high density, so the temperature index deteriorated regularly with increasing density. According to Figure 12 (b), when the pig density increased from 1.0 head/㎡ to 2.5 head/㎡, the energy consumption of the wet curtain increased from 24.5 kWh/day to 29.0 kWh/day, the energy consumption of the fan increased from 31.2 kWh/day to 40.5 kWh/day, and the total energy consumption increased from 55.7 kWh/day to 69.5 kWh/day. The reason is that the increase in density leads to an increase in metabolic heat that needs to be discharged inside the building. To maintain a suitable temperature, the wet curtain needed to lower the inlet water temperature to enhance the cooling effect, and the fan needed to increase the wind speed to accelerate heat dissipation. The increase in operating intensity of both led to an increase in energy consumption. The improved NFO algorithm was based on an energy-saving priority strategy, optimizing equipment parameters while meeting temperature requirements, so that the energy consumption increase matched the density increase, reflecting the algorithm's ability to balance energy consumption regulation under dynamic loads.

5.Conclusion

In response to the problems of high energy consumption, low accuracy, and difficulty in balancing temperature uniformity and energy-saving requirements in traditional methods of temperature control in pigsty environments, the research constructed a CFD approximate model based on Elman-NN, combined with an improved NFO algorithm, with the goal of improving temperature control efficiency and energy saving level through intelligent optimization strategies. The results show that under the outdoor scenario of 35°C and 1.5 pigs/sq m, the temperature MAE of the research method is 0.18°C, RMSE is 0.25°C, the daily energy consumption of a single pig house system is 68.9kWh, the temperature difference coefficient is 1.1, and the response time is 140s, which are better than PID, MPC and traditional GA+CFD. When the density of pigs increased from 1.0 head/㎡ to 2.5 head/㎡, the energy consumption of wet curtains increased from 24.5kWh/day to 29.0kWh/day, the energy consumption of fans increased from 31.2kWh/day to 40.5kWh/day, and the temperature uniformity index increased from 0.8 to 1.3. Research results denote that this method can effectively balance the temperature control accuracy and energy consumption of pig houses, and improve the intelligence level of environmental regulation. However, the study lacked long-term operational testing under extreme seasonal climates, failing to validate the system's stability in extreme conditions like severe cold and scorching heat. It also neglected to consider how equipment failures affect control performance and lacked a fault response mechanism. The system will be expanded to multi-season full-cycle testing, covering extreme temperature ranges from-15°C to-5°C in winter and 38°C to 42°C in summer, combined with humidity levels between 40% and 85%, to evaluate system adaptability. Additionally, an equipment fault warning module will be integrated to monitor real-time current and voltage of wet curtain pumps and fans, enabling early fault detection. This further enhances system practicality and stability, providing robust support for temperature control in large-scale livestock farming.

Fundings

The research is supported by: Xinjiang 'Tianchi Talents' Introduction Programme Funding Project, Research on Intelligent Management and Control System for Livestock and Poultry Breeding Environment Based on Wireless Sensing Technology, (Letter from the Xinjiang Department of Human Resources and Social Security [2024] No. 57) (NO. 2023TCLJ03); Scientific Research Project for High-level Talents of Xinjiang Institute of Technology, Research on Apple Sorting System Based on Deep Learning, (NO. XJLG2023G007).

Conflicts of Interest

The authors declare that they have no conflicts of interest.

Data Availability

The data used to support the findings of the research are available from the corresponding author upon reasonable request.

Author Contribution

SDY: study design, data collection, statistical analysis, visualization, writing, and revision of the original draft. WY revised the manuscript. GPW led and supervised this study. The final draft was verified by all authors before submission.

References

[1] M. Babaelahi and M. Lotfalipour. "Multi-objective optimization and comprehensive Thermodynamic, economic, and environmental analysis of an innovative solar-geothermal integrated system for synergistic power generation and water desalination," Energy Sources A: Recovery Util. Environ. Eff., vol. 46, no. 1, pp. 13065-13087, January, 2024, DOI: 10.1080/15567036.2024.2397502.

[2] J. Ge. "Research on Economic Environment Scheduling Optimization of Power System Based on Multi-objective Particle Swarm Optimization," Process Integr. Optim. Sustain., vol. 9, no. 1, pp. 275-290, January, 2025, DOI: 10.1007/s41660-024-00468-6.

[3] H. Yang. "Research on Multisensor Data Fusion Model for Monitoring Animal Breeding Environment," Automat. Contr. Comp. Sci., vol. 58, no. 1, pp. 23-32, June, 2024, DOI: 10.3103/S0146411624010103.

[4] T. Wang, G. Xi, Z. Sun and H. Zhu. "The prediction of external flow field and hydrodynamic force with limited data using deep neural network," J. Hydrodynamics, vol. 35, no. 3, pp. 549-570, March, 2023, DOI: 10.1007/s42241-023-0042-y.

[5] F. Jiang, C. Lin, J. Chen and C. Wu. "Energy consumption optimization method of wireless

sensor information collection network for new energy scheduling," J. Intell. Fuzzy Syst., vol. 45, no. 1, pp. 1743-1756, January, 2023, DOI: 10.3233/JIFS-222980.
[6] D. Ding, H. Yang, J. Liu, D. Zhang and X. Jiang. "Energy-saving optimization on active disturbance rejection decoupling multivariable control," Nucl. Eng. Technol., vol. 55, no. 3, pp. 850-860, March, 2023, DOI: 10.1016/j.net.2022.11.013.
[7] J. Lin, W. Lin, W. Lin, T. Liu, J. Wang and H. Jiang. "Multi-objective cooling control optimization for air-liquid cooled data centers using TCN-BiGRU-Attention-based thermal prediction models," Build. Simul., vol. 17, no. 12, pp. 2145-2161, December, 2024, DOI: 10.1007/s12273-024-1185-7.
[8] T. M. K. Mohamed, J. Gao and M. Tunio. "Development and experiment of the intelligent control system for rhizosphere temperature of aeroponic lettuce via the Internet of Things," Int. J. Agric. Biol. Eng., vol. 15, no. 3, pp. 225-233, March, 2022, DOI: 10.25165/j.ijabe.20221503.6530.
[9] L. Wang, Y. Zhang, M. Xu, Q. Liu and B. Wang. "Predictive control for greenhouse temperature and humidity and energy optimization by improved NMPC objective function algorithm," Int. J. Agric. Biol. Eng., vol. 17, no. 5, pp. 128-136, May, 2024, DOI: 10.25165/j.ijabe.20241705.8241.
[10] H. Y. Riskiawan, N. Gupta, D. P. S. Setyohadi, S. Anwar, A. A. Kurniasari, B. Hariono, M. H. Firmansyah, Y. Yogiswara, A. B. F. Mansur and A. H. Basori. "Artificial Intelligence Enabled Smart Monitoring and Controlling of IoT-Green House," Arab. J. Sci. Eng., vol. 49, no. 3, pp. 3043-3061, March, 2024, DOI: 10.1007/s13369-023-07887-6.
[11] A. Zaguia. "Smart greenhouse management system with cloud-based platform and IoT sensors," Spatial Inf. Res., vol. 31, no. 5, pp. 559-571, May, 2023, DOI: 10.1007/s41324-023-00523-3.
[12] J. Zhu, B. Sun, S. Pu, X. Pan, S. Xu, B. Hu and R. Qi. "Prediction model of temperature and humidity in pig barn based on multi-environmental factors analysis," J. South China Agric. Univ., vol. 45, no. 5, pp. 709-721, May, 2024, DOI: 10.7671/j.issn.1001-411X.202405017.
[13] S. Li, Q. Luo and Y. Zhou. "Enhanced Multi-Object Dwarf Mongoose Algorithm for Optimization Stochastic Data Fusion Wireless Sensor Network Deployment," Comput. Model. Eng. Sci., vol. 142, no. 2, pp. 1955-1994, February, 2025, DOI: 10.32604/cmes.2025.059738.
[14] R. Xing, M. Li, C. Dai, P. Xu, J. Zhang, H. Wang, W. Wang and Z. Hu. "Study on dynamic control system of tunnel variable air volume ventilation based on first-order delay and predictive compensation control model," J. Eng. Res., vol. 13, no. 2, pp. 1449-1461, February, 2025, DOI: 10.1016/j.jer.2023.11.012.
[15] H. Yang. "Research and Implementation of Intelligent Monitoring and Evaluation System for Farm Animals Breeding Environment," Automat. Contr. Comp. Sci., vol. 57, no. 4, pp. 355-363, March, 2023, DOI: 10.3103/S0146411623040090.
[16] V. Dhakane and A. Yadav. "Computational Fluid Dynamics-Deep Neural Network (CFD-DNN) Surrogate Model with Graphical User Interface (GUI) for Predicting Hydrodynamic Parameters in Three-Phase Bubble Column Reactors," Ind. Eng. Chem. Res., vol. 63, no. 26, pp. 11670-11685, June, 2024, DOI: 10.1021/acs.iecr.4c00669.
[17] A. N. Ramli and M. F. F. Ab Rashid. "Assembly Line Balancing with Energy Consumption Optimization Using Substituted Tiki-Taka Algorithm," Process Integr. Optim. Sustain., vol. 8, no. 4, pp. 1065-1079, April, 2024, DOI: 10.1007/s41660-024-00413-7.
[18] W. Alayed, A. Akhtar, W. U. Hassan and A. Zeeshan. "Maximizing energy savings in smart

homes through artificial neural network-based artificial intelligence solutions," Clean Energy, vol. 9, no. 2, pp. 140-149, February, 2025, DOI: 10.1093/ce/zkae113.
[19] S. Zhang, Z. Nie, S. Chen and L. Zhao. "Adaptive blind control strategy based on iterative optimization to minimize cooling and lighting demands in office space," Build. Simul., vol. 18, no. 1, pp. 207-223, January, 2025, DOI: 10.1007/s12273-024-1211-9.
[20] C. Guo, L. Zhang and C. Peng. "Research and Application of Energy Consumption Optimization Design of Electromechanical System Based on Genetic Algorithms," J. Ind. Manag. Optim., vol. 20, no. 10, pp. 3265-3290, October, 2024, DOI: 10.3934/jimo.2024053.
[21] Z. Huang and S. Wang. "Joint Visual Coverage and Energy Consumption Optimization for UAV-Aided 5G-and-Beyond Communications," IEEE Trans. Veh. Technol., vol. 73, no. 12, pp. 19417-19431, December, 2024, DOI: 10.1109/TVT.2024.3433606.
[22] L. Yang, H. Zhang, J. Zhang and X. Yue. "Optimization analysis of distributed energy consumption based on dynamic data synchronization and intelligent control," Int. J. Adapt. Control Signal Process., vol. 38, no. 7, pp. 2502-2519, July, 2024, DOI: 10.1002/acs.3815.
[23] R. Jose and K. Srinivasan. "Multi-Objective Modeling Framework for Environmental Flow Optimization in a River-Reservoir System Using Histogram Comparison Approach for Estimation of Hydrologic Alteration," Water Resour. Manag., vol. 39, no. 1, pp. 439-458, January, 2025, DOI: 10.1007/s11269-024-03977-8.
[24] G. Zhang, Y. Du, X. Zhu and X. Liu. "Hybrid Operator and Strengthened Diversity Improving for Multimodal Multi-Objective Optimization," Tsinghua Sci. Technol., vol. 29, no. 5, pp. 1409-1421, May, 2024, DOI: 10.26599/TST.2023.9010123.
[25] Z. Wang, X. Chen, J. Yan and J. Liu. "An intelligent mesh-smoothing method with graph neural networks," Front. Inf. Technol. Electron. Eng., vol. 26, no. 3, pp. 367-384, March, 2025, DOI: 10.1631/FITEE.2300878.
[26] Y. Liu, G. Gao and W. Zhao. "Risk-Averse Distributionally Robust Environmental-Economic Dispatch Strategy Based on Renewable Energy Operation: A New Improved Whale Optimization Algorithm," IEEJ Trans. Electr. Electron. Eng., vol. 20, no. 5, pp. 696-711, May, 2025, DOI: 10.1002/tee.24239.
[27] J. Liu, B. Zhang, Y. Lai and L. Fang. "Hull form optimization research based on multi-precision back-propagation neural network approximation model," Int. J. Numer. Methods Fluids, vol. 96, no. 8, pp. 1445-1460, August, 2024, DOI: 10.1002/fld.5291.
[28] G. Calzolari and W. Liu. "Deep learning to develop zero-equation based turbulence model for CFD simulations of the built environment," Build. Simul., vol. 17, no. 3, pp. 399-414, March, 2024, DOI: 10.1007/s12273-023-1083-4.
[29] G. Ortali, A. Gabbana, I. Atmodimedjo and A. Corbetta. "Enhancing Lattice Kinetic Schemes for Fluid Dynamics with Lattice-Equivariant Neural Networks," AIAA J., vol. 63, no. 2, pp. 716-731, February, 2025, DOI: 10.2514/1.J064453.
[30] C. Hebbi and H. Mamatha. "Comprehensive Dataset Building and Recognition of Isolated Handwritten Kannada Characters Using Machine Learning Models," Artif. Intell. Appl., vol. 1, no. 3, pp. 179-190, March, 2023, DOI: 10.47852/bonviewAIA3202624.

Submitted: 02.09.2025.
Revised: 18.10.2025.
Accept: 05.11.2025.